4.
WATER-LOADED METAL-DIELECTRIC WALL DIAGONAL HORN TERMINATED IN BIO-MEDIUM/BIO-MEDIA

4.1 Introduction

Water-loaded conventional metal diagonal horn (MDH) provides circularly symmetric heating pattern, but penetration depth (PD) in the biological media is not good enough. Therefore, it is thought to modify the aperture field distribution of the water-loaded conventional MDH without changing its aperture size in order to obtain enhanced PD in addition to symmetric effective field size (EFS) in the biological media. Considering these aspects, the author proposed a new metal-dielectric wall diagonal horn (MDWDH). The proposed horn is a new form of conventional diagonal horn [Love (1976)] in which the major portions of the antenna walls in the central regions are made of dielectric material (Perspex) while remaining wall portions are made of metal, considering the region of the antenna from throat to aperture. In other words, the new diagonal horn is a modified version of conventional MDH. Due to partial replacement of metal-walls with dielectric walls in the conventional MDH, the field distribution over the aperture of new diagonal horn is a closer approximation to the uniform distribution that may ensure uniform absorbed-power distribution in bio-medium/media and prevent steep power gradient in the bio-medium/media.

In this chapter, new MDWDH antennas terminated in biological (muscle) phantom/tri-layered bio-media without/with realistic oval-/irregular-shaped tumor have been investigated through simulation and experimentally at 2450 MHz and through simulation at 915 MHz for hyperthermia application. The new diagonal horn is filled with water to provide good impedance match between the horn and bio-medium/media, which ensures good transmission into the bio-medium/media.

4.2 Design and/or fabrication of water-loaded metal-dielectric wall diagonal horns (MDWDHs)

Direct-contact water-loaded MDWDHs were designed at 2450 and 915 MHz by applying basic design principles of corresponding water-loaded conventional

MDHs and optimized using computer simulation technology microwave studio (CST MWS) 2011 software. Further, the horn designed at 2450 MHz is fabricated to demonstrate the technical feasibility of the horn. Geometry of proposed water-loaded MDWDHs for operation at ISM frequencies of 2450 and 915 MHz is shown in Figure 4.1. The basic idea of designing the proposed MDWDH has been taken from reference [Van Rhoon *et al.* (1998)] in which the E-plane side walls of a metal (brass) pyramidal horn carrying TE_{10} mode are replaced by Lucite dielectric (ε_r = 2.59 - j0.022). However, in the conventional MDH antenna, the fields correspond to two orthogonal modes (TE_{10} and TE_{01}) [Love (1976)]. Therefore, in the design of MDWDH, the central portions of all the four walls of the conventional MDH are replaced by Perspex dielectric to enhance the PD and to some extent EFS also without degrading the ruggedness of the antenna significantly. The enhancement in PD and EFS in the bio-medium due to each MDWDH is made possible due to the generation of hybrid modes in the antenna, which makes the field distribution across its aperture more uniform.

As shown in Figure 4.1, corresponding water-loaded metal rectangular guide carrying TE_{10} mode for each horn is gradually transformed to circular guide carrying the TE_{11} mode. Another gradual transition converts the circular metal cross section into square metal cross-section. Each MDWDHs with its walls made of copper (conductor) and Perspex dielectric combination then flares out from the throat square cross-section to the desired aperture size. The central portions of the walls from throat to aperture of the MDWDHs designed at 2450 and 915 MHz are made of Perspex dielectric (ε_r' = 2.59) and the remaining wall portions are of copper conductor as shown in Figure 4.1. Same thickness (= 2 mm) of Perspex dielectric and copper conductor is taken in forming the walls of these MDWDHs. The dimensions of Perspex and metal (copper) portions of walls of each antenna were optimized through simulation to obtain maximum depth of penetration in the phantom bio-medium, which is in direct contact with the antenna aperture at the operating frequency. The dimensional details of the MDWDHs designed at 2450 and 915 MHz are provided in Table 4.1. The presence of dielectric in a portion of each wall of the MDWDH generates hybrid modes.

The aperture of each MDWDHs is assumed to be surrounded by a conducting ground plane of copper in xy-plane so that the fringing electric field outside the aperture becomes zero. The dimensions of the conducting ground plane are 150 mm ×150 mm × 2 mm, and 250 mm × 250 mm × 2 mm for the MDWDHs designed at 2450 and 915 MHz respectively.

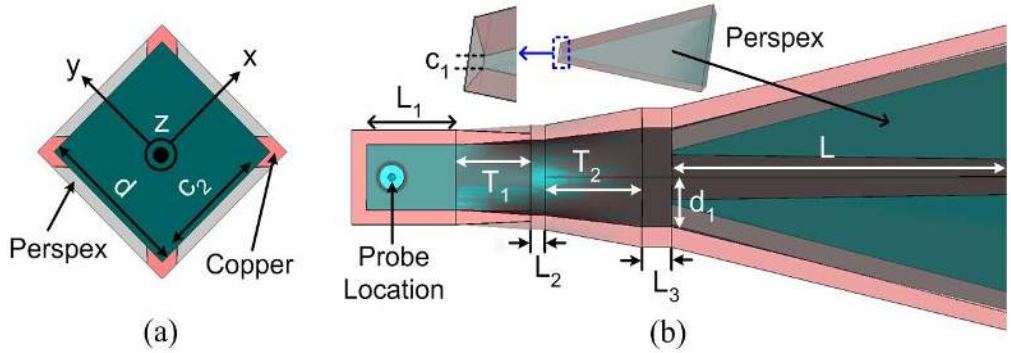

Figure 4.1: Geometry of water-loaded MDWDH antenna (a) top view, and (b) side view.

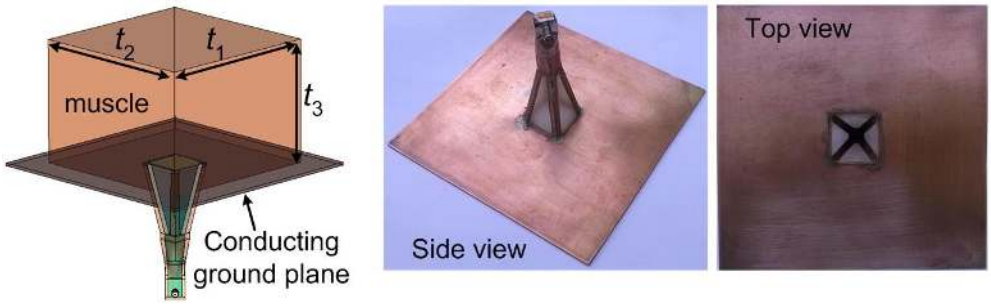

Figure 4.2: (a) Water-loaded MDWDH antenna terminated in bio-medium and (b) Fabricated antenna for study at 2450 MHz.

Table 4.1: Dimensional details of the water-loaded MDWDHs

Parameter	Symbol	Dimension (mm)	
		2450 MHz	915 MHz
Length of input waveguide	L_1	12	20
Transition length of circular	T_1	10	12
Length of circular waveguide	L_2	2	2
Diameter of circular waveguide	D	10	33.4
Transition length of square	T_2	13	12
Length of square waveguide	L_3	4	3
Throat size	d_1	9.2	29
Length of flaring section	L	46	106
Aperture size	d	24.6	65
Width of Perspex at the throat	c_1	0.8	8
Width of Perspex at the aperture	c_2	18	48

The dimension optimization of the MDWDHs including the width of the Perspex dielectric material was carried out through simulation. The optimized dimensions of the MDWDHs are given in Table 4.1. A 3D-view of water-loaded MDWDHs terminated in phantom bio-medium is shown in Figure 4.2(a). Figure 4.2(b) shows different views of the fabricated version of the proposed MDWDH for operation at 2450 MHz.

4.3 Water-loaded metal-dielectric wall diagonal horn (MDWDH) terminated in phantom muscle

To study the modification of aperture field distributions of water-loaded MDWDHs designed at 2450 and 915 MHz due to the presence of partial dielectric material on the walls of the horns, and the resulting SAR distributions in phantom muscle due to these horns, simulation was performed. In addition, experimental study of SAR distribution in phantom muscle due to the horn designed at 2450 MHz was also carried out. The simulation results for SAR distribution in the phantom bio-medium at 2450 MHz are also compared with the experimental distribution. The simulation of aperture field distributions of both the horn antennas and SAR distributions in phantom muscle due to these antennas was carried out using CST MWS software. The experimental study of SAR distributions in the phantom bio-medium of known physical properties [Stuchly and Stuchly (1980)] was carried out at 2450 MHz with the help of Vidyut Yantra make 50 Ω coaxial L-shaped and straight monopole probes and Agilent make spectrum analyser (Model E4448A). The frequency of 2450 MHz was chosen for experimental study because of the availability of respective equipment components in the laboratory and also to verify the results with those obtained through simulation.

4.3.1 *Results and discussion*

4.3.1.1 *Applicators' characteristics*

The applicator's design data and dielectric property of phantom muscle medium given in sections 4.2 and 4.3 have been used to obtain the simulated values of input reflection coefficient of the MDWDH antennas designed at 2450

and 915 MHz, each in direct contact with the phantom muscle medium. The simulated values of input reflection coefficient of the antenna terminated in the phantom muscle medium are -19 dB and -22 dB respectively at the operating frequencies of 2450 and 915 MHz. Further, measured input reflection coefficient of the applicator designed at 2450 MHz and terminated in phantom muscle medium is -12 dB.

4.3.1.2 *Simulated electric field distributions*

The effective heating of the biological phantom depends strongly on the size of the antenna aperture and the field distribution across it. Figures 4.3(a) and 4.4(a) depict the simulated electric field distributions over the apertures of the conventional MDHs designed at 2450 and 915 MHz. It can be seen from Figures 4.3(a) and 4.4(a) that in the absence of partial dielectric plates (in case of conventional MDHs), the amplitude of electric field intensity goes down near the periphery of each horn due to propagation of only TE_{10} and TE_{01} modes.

The effect of the replacing the portions of the walls near the corners of water-loaded conventional MDHs with Perspex dielectric on their respective aperture field distributions was studied through simulation. Figures 4.3(b) and 4.4(b) show the aperture field distributions of the antennas in which wall portions near the corners of the respective conventional MDHs are replaced by dielectric material. It can be observed from Figures 4.3(b) and 4.4(b) that frequency dependent effect on aperture field distribution is observed when Perspex is placed near the corners of the horn walls of the antennas. This effect is caused due to the generation of hybrid modes in the antennas.

Figures 4.3(c) and 4.4(c) show the simulated aperture field distributions of the proposed MDWDHs at 2450 and 915 MHz. In the MDWDHs, the central portions of all the four walls of the corresponding conventional MDHs are replaced by Perspex dielectric and the widths of the dielectric at the throat and aperture are designated as c_1 and c_2 respectively (Figure 4.1). The enhancement of aperture field near the corners of the MDWDHs can be observed from Figures 4.3(c) and 4.4(c). Therefore, the simulated electric field distributions across the

apertures of new horns have become more uniform as compared with the corresponding conventional MDHs (chapter 2) of same sizes.

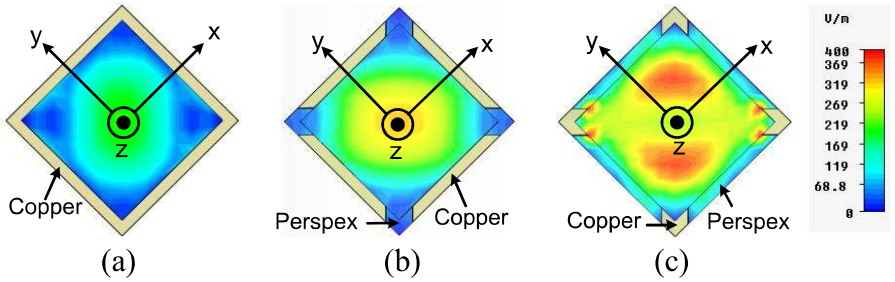

(a) (b) (c)

Figure 4.3: Simulated field distributions for 2450 MHz at the aperture of (a) conventional MDH, (b) the horn with Perspex near the corners of antenna walls, and (c) the proposed MDWDH.

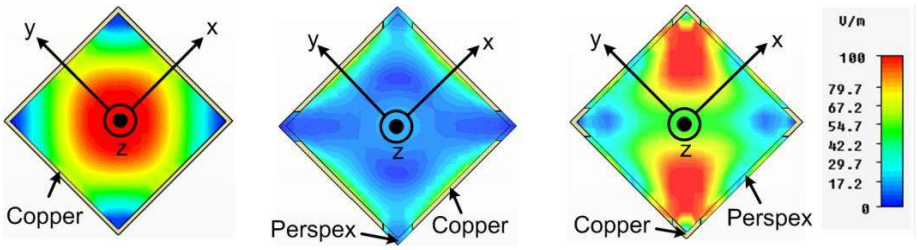

(a) (b) (c)

Figure 4.4: Simulated field distributions for 915 MHz at the aperture of (a) conventional MDH, (b) the horn with Perspex near the corners of the antenna walls, and (c) the proposed MDWDH.

4.3.1.3 *SAR distributions in phantom muscle medium*

4.3.1.3.1 *Simulated SAR distributions at 2450 and 915 MHz*

The density and conductivity of the phantom muscle medium used in simulation study of SAR distributions are given in Table 4.3. The simulated relative SAR distributions inside the phantom bio-medium (muscle) of size $t_1 \times t_2 \times t_3$ = 112 mm × 112 mm × 80 mm and 200 mm × 200 mm × 150 mm due to the MDWDHs designed at 2450 and 915 MHz respectively are determined and the results are shown in Figures 4.5–4.7. The simulation results given in Figure 4.7 correspond to the optimized antennas. Initially, the power fed to the antenna was assumed to be 1W in the simulation study. The relative SAR distributions in the biological phantom are obtained by normalizing the SAR values with respect to the respective maximum value of SAR that occurs in the biological phantom at each frequency.

Effect of presence of partial dielectric material in the horn walls on SAR

Dielectric material located in the central portions of the antenna walls plays an important role in modifying the aperture field distribution and hence the SAR distribution in the bio-medium. In order to evaluate the effect of the presence of dielectric plates along with metal plates in the walls of MDWDH on SAR distribution, parametric study was carried out through simulation at 2450 MHz.

Figure 4.5(a) shows the effect of dielectric dimension (c_1) at the throat of the MDWDH on the relative SAR distribution in the biological phantom at 2450 MHz. It is clear from Figure 4.5(a) that PD in the phantom muscle medium decreases as the value of c_1 is altered from the optimum value of 0.8 mm. The optimum value of c_1 (= 0.8 mm) provides maximum PD and appropriate peak SAR value.

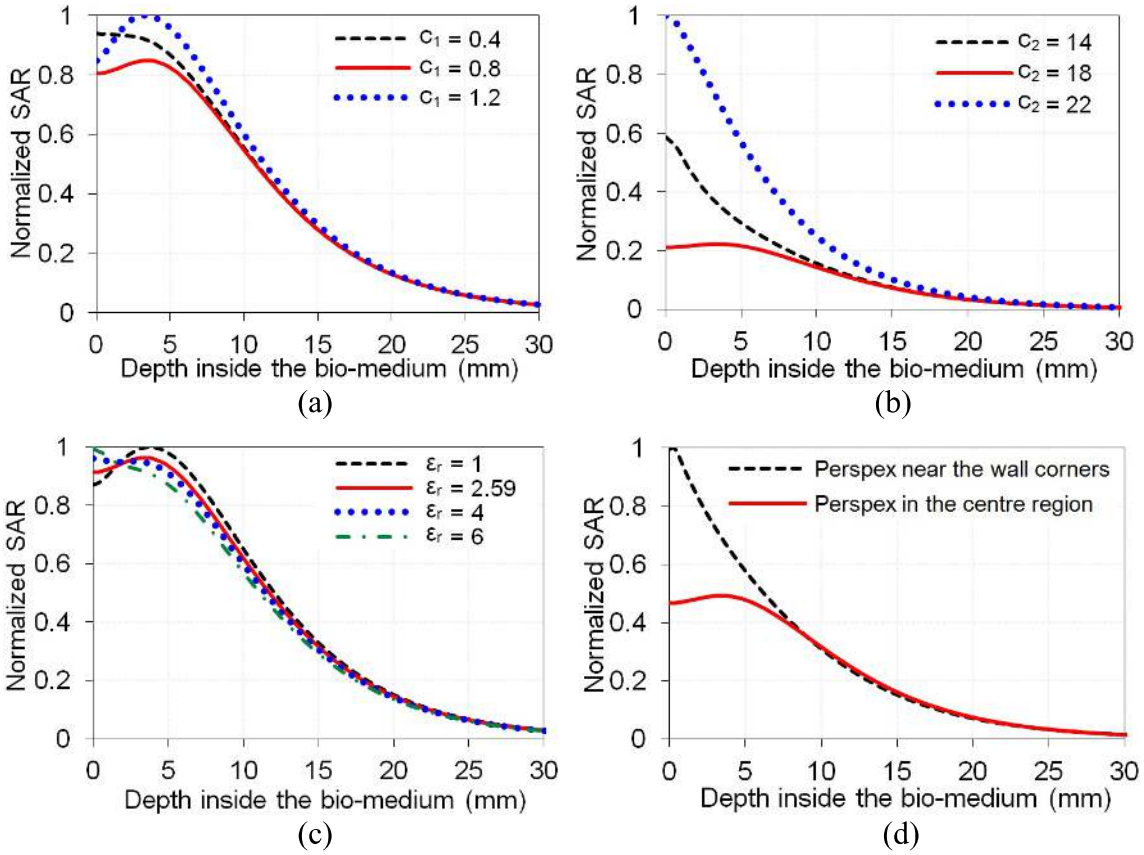

Figure 4.5: Effects of dielectric location, its dielectric property, dimensions (a) c_1, (b) c_2, and (c) dielectric constant value, and (d) location of dielectric material on normalized SAR distributions along z-direction in phantom muscle due to the MDWDH at 2450 MHz.

Figure 4.5(b) illustrates the effect of dielectric dimension (c_2) at the aperture of the MDWDH on the relative SAR distribution in the biological phantom at

2450 MHz. It can be observed from Figure 4.5(b) that as we change the value of dielectric dimension c_2 at the aperture of the MDWDH from the optimum value of 18 mm, peak relative SAR in the biological phantom increases and slight reduction in the value of PD occurs. Figure 4.5(c) depicts the effect of change in dielectric constant (ε_r) of the dielectric material on the relative SAR distribution in the phantom muscle at 2450 MHz. It is observed from Figure 4.5(c) that a slight variation in the value of peak SAR occurs, as we change the value of ε_r.

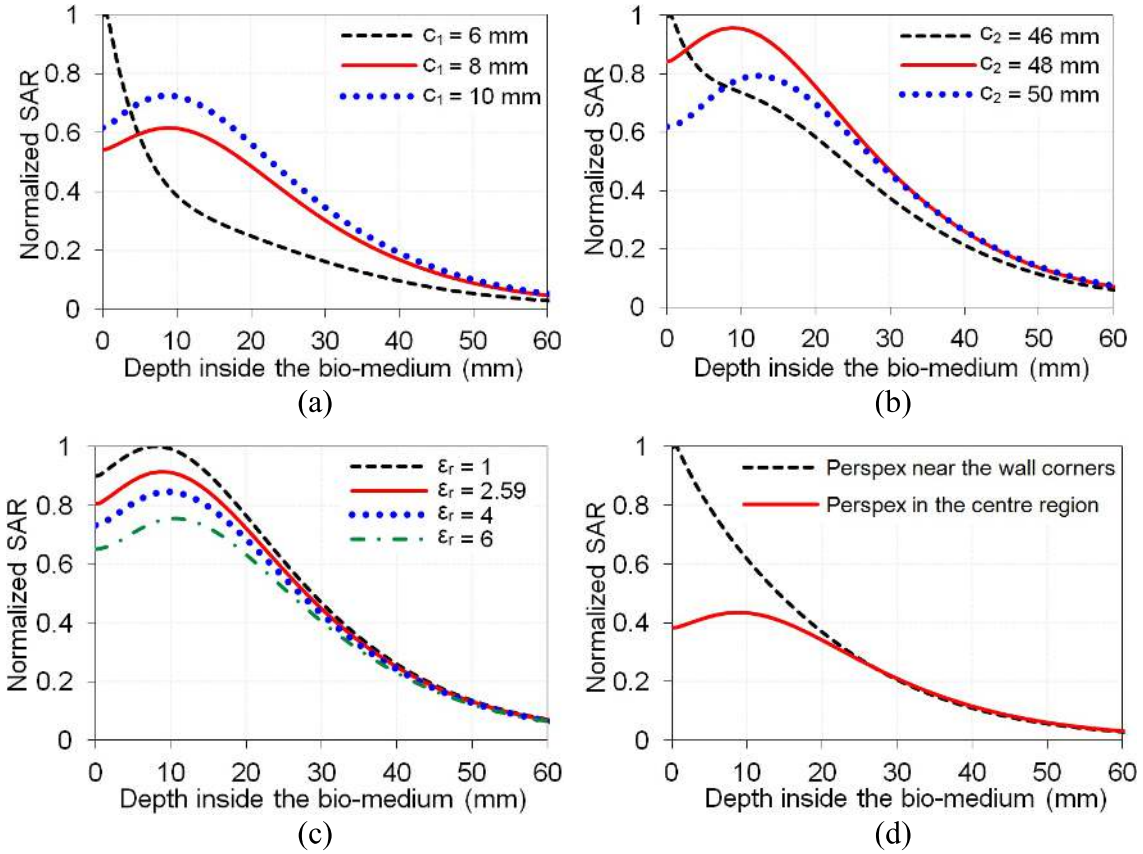

Figure 4.6: Effects of dielectric location, its dielectric property, dimensions (a) c_1, (b) c_2, and (c) dielectric constant value, and (d) location of dielectric material on normalized SAR distributions along z-direction in phantom muscle due to the MDWDH at 915 MHz.

Figure 4.5(d) shows the effect of change in the position of dielectric material in the antenna walls on relative SAR distribution in the biological phantom at 2450 MHz. It is clear from Figure 4.5(d) that as we shift the position of dielectric plates from central region of the walls to the corners regions, an enhancement in the value of peak SAR and reduction in PD are obtained. It is to be noted that the values of peak absolute SAR used for normalization of SAR distribution curves

given in Figure 4.5(a), (b), (c) and (d) for the MDWDH designed at 2450 MHz are respectively equal to 71.6, 271.8, 62.9 and 123.2 W/kg.

Similar arguments apply for the MDWDH designed at 915 MHz and the variation of relative SAR distributions in the phantom muscle medium due to the applicator at 915 MHz for the values of c_1, c_2, dielectric constant (ε_r) of the dielectric material and change in the position of dielectric material in the antenna walls are also given in Figures 4.6(a), 4.6(b), 4.6(c) and 4.6(d). Similarly, the values of peak absolute SAR used for normalization of SAR distribution curves given in Figure 4.5(a), (b), (c) and (d) for the MDWDH designed at 915 MHz are respectively equal to 7.1, 4.6, 4.79 and 10.1 W/kg.

4.3.1.3.2 *Experimental SAR distribution in phantom muscle medium at 2450 MHz*

The relative SAR distributions in the phantom muscle medium due to the optimized MDWDH designed at 2450 MHz were measured to verify the experimental results with those obtained through simulation. Relative SAR distributions inside the phantom muscle of size 112 mm × 112 mm × 80 mm were determined experimentally following the procedure given in chapter 2. The measured relative SAR distributions in the phantom muscle due to the optimized MDWDH at 2450 MHz are given in Figure 4.7. The relative SAR distributions were determined experimentally at 2450 MHz because of (i) to verify the results obtained through simulation, and (ii) the availability of equipments/components at 2450 MHz in our laboratory.

4.3.1.3.3 *Comparison of simulated and/or experimental SAR distributions*

Figure 4.7(a) illustrates the relative SAR distributions in the homogeneous phantom muscle in z-direction for the optimized MDWDHs as well as for the respective conventional MDHs designed at 2450 and 915 MHz. Different curves of the relative SAR distributions were obtained by normalizing the absolute SAR values of the curves with respective peak absolute SAR values (reference values). That is why, value of maximum normalized SAR value for all described curves is identical. The values of simulated and/or experimental PD in biological phantom

(depth where relative SAR value is down to 13.5 percent of the maximum in the tissue) extracted from Figure 4.7(a) are given in Table 4.2. It can be seen from Table 4.2 that the measured PD in the biological phantom at 2450 MHz is nearly in agreement with the simulated value. Further, the simulated value of PD in the phantom bio-medium at 915 MHz is higher than the simulated value of PD in the bio-medium at 2450 MHz. In addition, the simulated values of PD in the bio-medium due to the proposed MDWDHs at 2450 and 915 MHz are higher than the values of PD due to corresponding conventional MDHs.

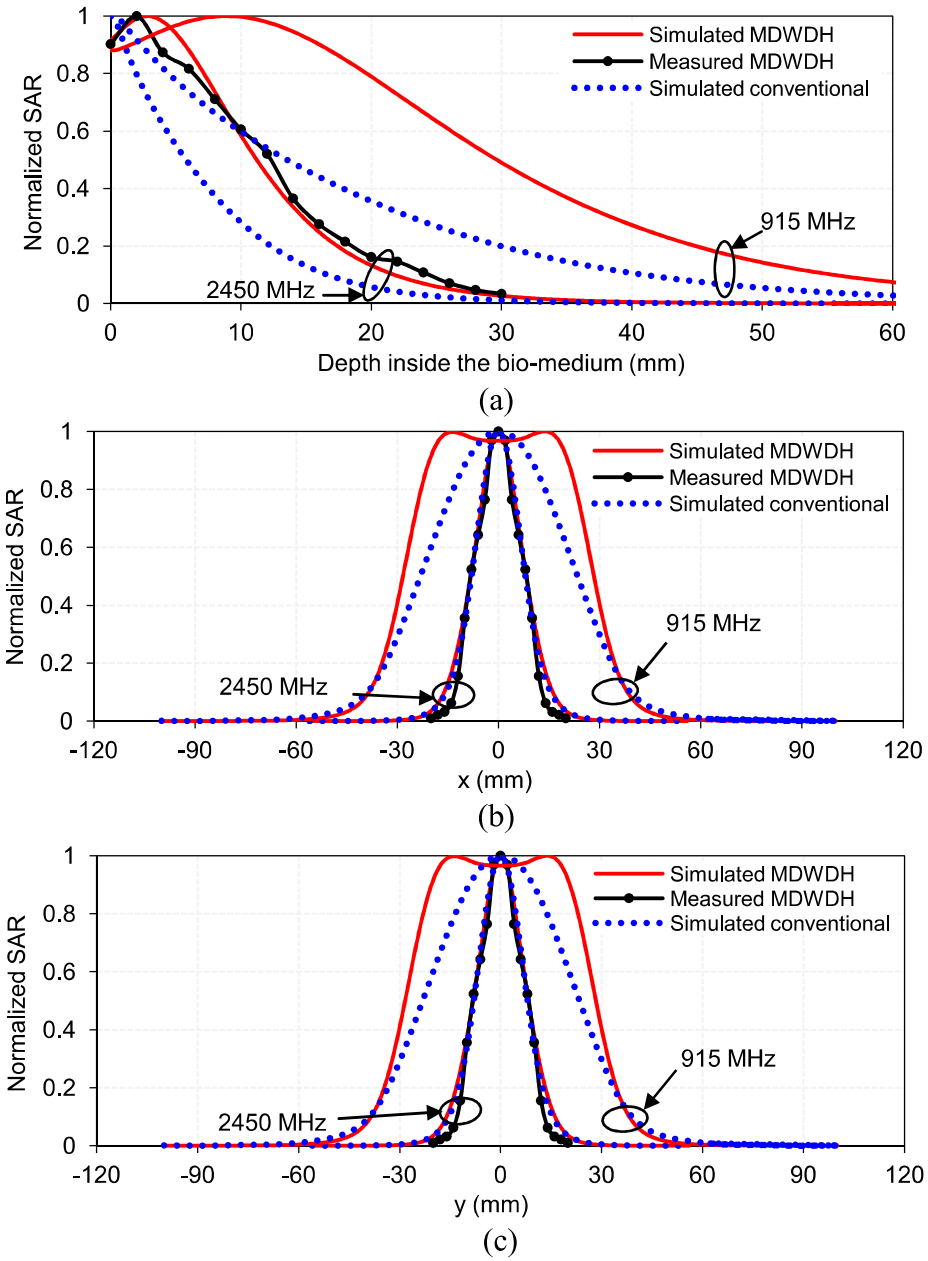

Figure 4.7: Normalized SAR distributions inside the phantom muscle due to MDWDH/Conventional MDH antennas at 2450 and 915 MHz along (a) z-direction (x = y = 0), (b) x-direction at z = 10 mm (y = 0), and (c) y-direction at z = 10 mm (x = 0).

The EFS is defined as the area that is enclosed within 50% SAR contour inside the phantom bio-medium. The simulated and/or experimental values of EFS in the homogeneous bio-medium extracted from Figures 4.7(b) and 4.7(c) due to the optimized MDWDHs as well as due to respective conventional MDHs designed at 2450 and 915 MHz are given in Table 4.2. It can be seen from Table 4.2 that measured and simulated values of EFS in the bio-medium at 2450 MHz are small, nearly in agreement with each other. Further, the simulated and/or measured values of EFS in the phantom bio-medium at 2450 and 915 MHz exhibit circular symmetry. The MDWDHs have almost identical aperture illuminations in E- and H-planes. That is why, they provide circularly symmetric SAR distribution in the transverse plane. In addition, it can be observed from Table 4.2 that simulated value of EFS in the bio-medium at 915 MHz is higher than the corresponding value at 2450 MHz. Also the simulated values of EFS due to the optimized MDWDH antennas at 2450 and 915 MHz are slightly higher than the respective values due to conventional MDH antennas.

Table 4.2: SAR Parameters due to the MDWDH/conventional MDH antennas terminated in homogeneous phantom bio-medium

SAR parameters			Frequency (MHz)	
			2450	915
PD (mm)	Simulated	MDWDH	20.6	53
		Conventional MDH	15	36
	Measured MDWDH		22	–
EFS (mm^2)	Simulated	MDWDH	17 × 17	57 × 57
		Conventional MDH	16 × 16	46 × 46
	Measured MDWDH		16 × 16	–

4.4 Simulation study on water-loaded MDWDH terminated in tri-layered bio-media without and with tumor

The work presented in preceding sections is extended by performing simulation study on two water-loaded MDWDHs (designed at 2450 and 915 MHz), each in direct contact with tri-layered bio-media (skin, fat and muscle layers) without and with embedded tumor for determination of SAR and temperature distributions using CST MWS software. The performance of each

horn is studied through simulation for three tri-layered bio-models (one without tumor, and the other two consisting of superficial irregular- and oval-shaped abdominal/limb tumors) lying inside the muscle tissue taken one at a time as shown in Figure 4.8. The locations of oval- and irregular-shaped tumors embedded within second and third tri-layered bio-models considered for each of the applicators designed at 2450 and 915 MHz are provided in Figure 4.9. In all, four tumors of different shapes/sizes (two for each of the applicators) were considered in the present study. For heating of tumors designated as tumor1 (oval-shaped) and tumor2 (irregular-shaped), water-loaded MDWDH designed at 2450 MHz which is in direct contact with tri-layered bio-media containing these tumors (one at a time) was considered. For heating of tumors designated as tumor3 (oval-shaped) and tumor4 (irregular-shaped), water-loaded MDWDH designed at 915 MHz which in direct contact with tri-layered bio-media containing the aforesaid tumors (one at a time) was considered. A cancerous tissue has higher water content [Michaelson and Lin (1987)] and therefore higher dielectric constant and conductivity. The values of complex relative permittivity, density and thickness of different layers of bio-media and tumors are same as those used in chapter 3.

4.4.1 *SAR distributions without and with tumor*

To observe the effect of tumor embedded in the muscle layer, simulations were performed for the MDWDH terminated in tri-layered bio-media with embedded tumor and the corresponding normalized SAR distributions are depicted in Figures 4.10–4.13.

Figures 4.10 and 4.11 show the simulated variations of normalized SAR distributions in the inhomogeneous tri-layered bio-media without/with embedded tumor, along z-direction (for x = y = 0) due to the MDWDHs designed at 2450 and 915 MHz respectively whereas Figures 4.12 and 4.13 show the variations of normalized SAR distributions in the aforesaid configurations of bio-media along x-/y-directions due to the MDWDHs designed at 2450 and 915 MHz respectively. The values of PD and EFS for the frequencies of 2450 MHz and 915 MHz extracted from Figures 4.10-4.13 are given in Table 4.3. It can be seen from Table

4.3 that the values of PD and EFS due to the MDWDHs are significantly higher at 915 MHz as compared to those at 2450 MHz. Further, the presence of a tumor does not alter PD and EFS (in the centre of tumor) significantly in each case. Also, relative SAR value observed at the skin surface using the water-loaded MDWDH applicator designed at 915 MHz is low. However, relative SAR value at the skin surface is high due to the water-loaded MDWDH applicator designed at 2450 MHz. Additionally, it is observed that PD in the tri-layered bio-model due to the water-loaded MDWDHs designed at 2450 and 915 MHz is sufficient to heat the respective tumor of whole depth effectively.

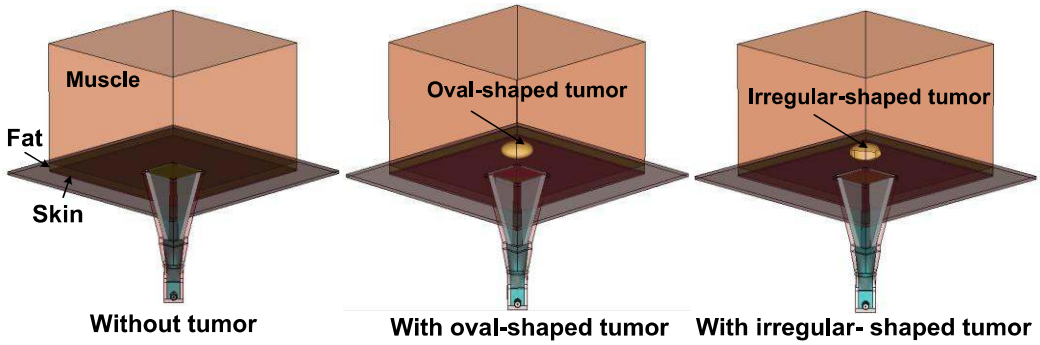

Figure 4.8: Metal-dielectric wall diagonal horn antenna designed at a given frequency and terminated in tri-layered bio-media.

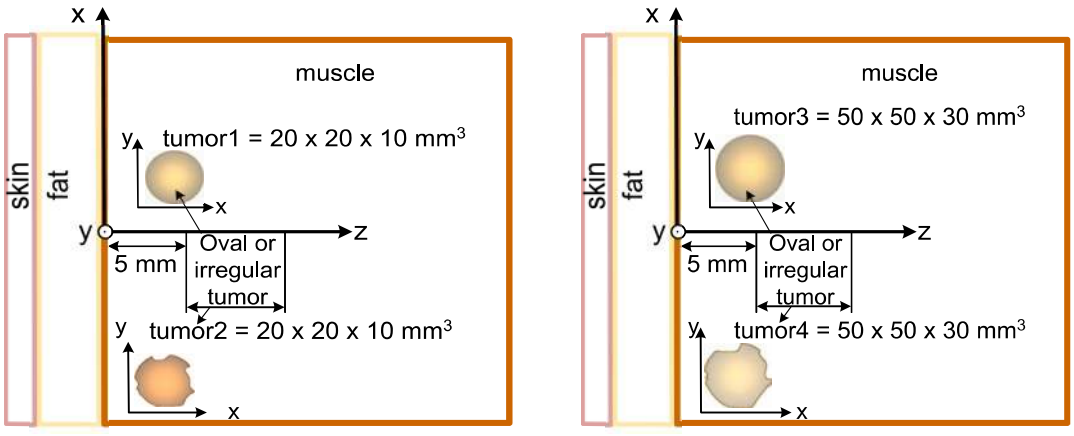

Figure 4.9: Two-dimensional realistic tri-layered bio-model with embedded (a) tumor1/tumor2 (applicable for the horn designed at 2450 MHz), and (b) tumor3/tumor4 (applicable for the horn designed at 915 MHz).

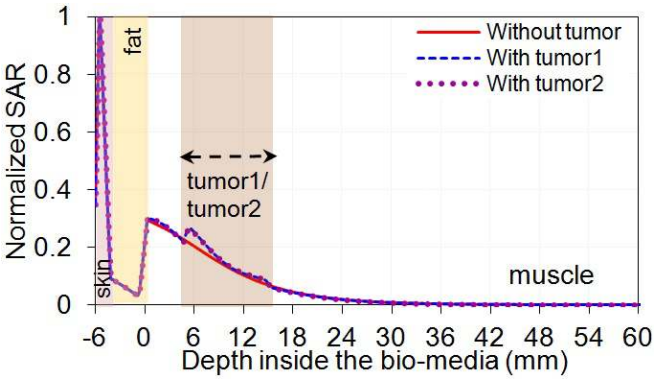

Figure 4.10: Simulated normalized SAR distributions inside the bio-model without and embedded tumor1/tumor2 due to MDWDH at 2450 MHz along z-direction (x = y = 0).

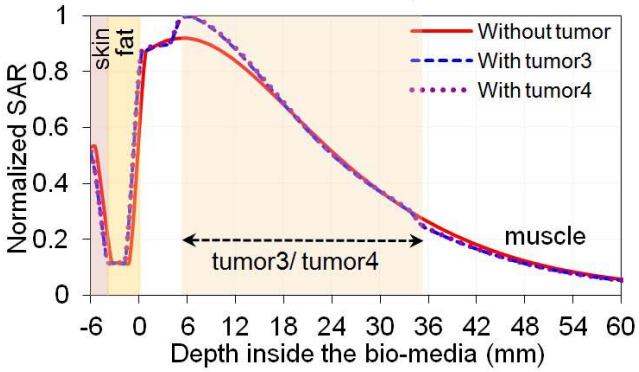

Figure 4.11: Simulated normalized SAR distributions inside the bio-model without and with embedded tumor3/tumor4 due to MDWDH at 915 MHz along z-direction (x = y = 0).

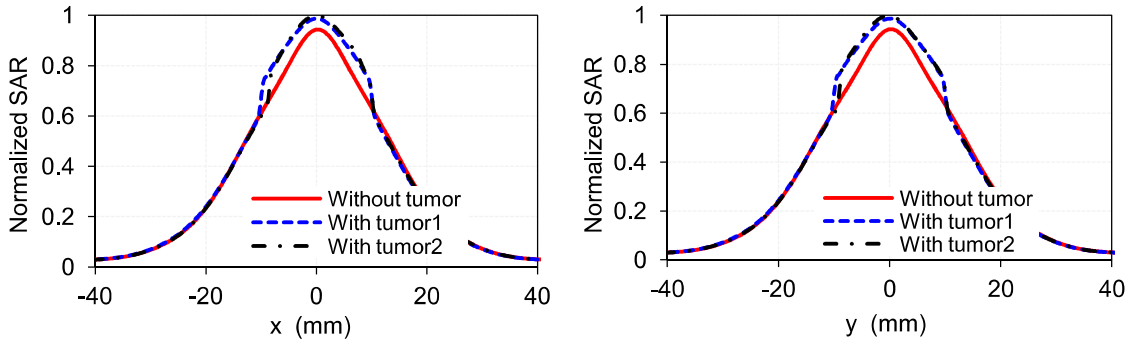

Figure 4.12: Simulated normalized SAR distributions inside the bio-models due to the MDWDH at 2450 MHz along (a) x-direction at z = 10 mm (middle of tumor1/tumor2) (y = 0), and (b) y-direction at z = 10 mm (middle of tumor1/tumor2) (x = 0).

4.4.2 *Temperature distributions without and with tumor*

In order to characterize the hyperthermia treatment system, inhomogeneous tri-layered bio-models fed through the water-loaded MDWDH were considered. The thermal simulation was performed by CST multi-physics simulator software

at an initial temperature of 37° C. The thermal parameters of the bio-models used in simulation are same as given in chapter 2.

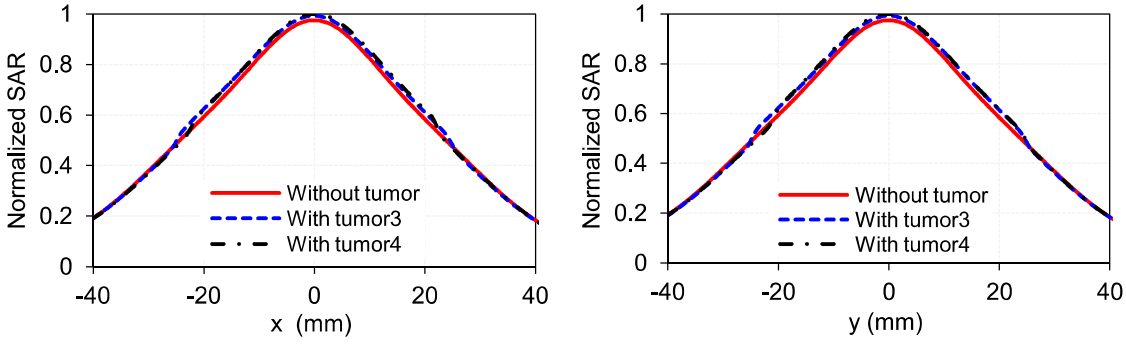

Figure 4.13: Simulated normalized SAR distributions inside the bio-models due to the MDWDH at 915 MHz along (a) x-direction at z = 20 mm (middle of tumor3/tumor4) (y = 0), and (b) y-direction at z = 20 mm (middle of tumor3/tumor4) (x = 0).

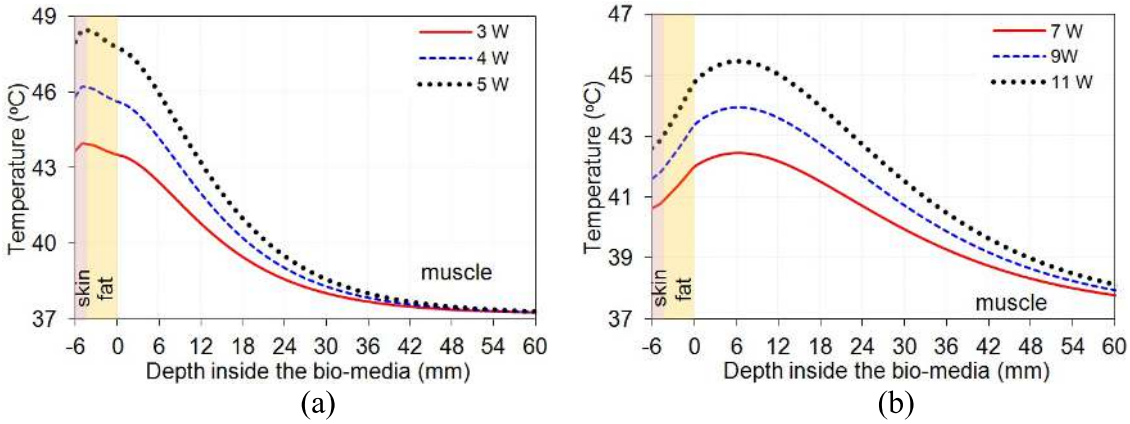

Figure 4.14: Temperature distribution inside the tri-layered bio-media without tumor for different input power levels along z-direction (x=y=0) due to the MDWDH at (a) 2450 MHz and (b) 915 MHz.

Figure 4.14(a) and (b) shows the variations of temperature as a function of depth in the tri-layered bio-model without tumor due to the MDWDHs designed at 2450 MHz and 915 MHz respectively by taking input power level as a parameter. It can be seen from Figure 4.14 that as the power fed to the applicator at a given frequency increases, the temperature in the bio-media rises. Further, higher power level is required at lower frequency to obtain a given tissue temperature at particular depth within the distance range along z-direction encompassing PD. As expected, the temperature in each case decreases exponentially with depth inside the bio-media. It can be inferred from Figure 4.14 that the desired temperature

range (41-45 ^{o}C) for effective hyperthermia was achieved for input power levels of 4 and 9 W for the applicators designed at 2450 and 915 MHz respectively.

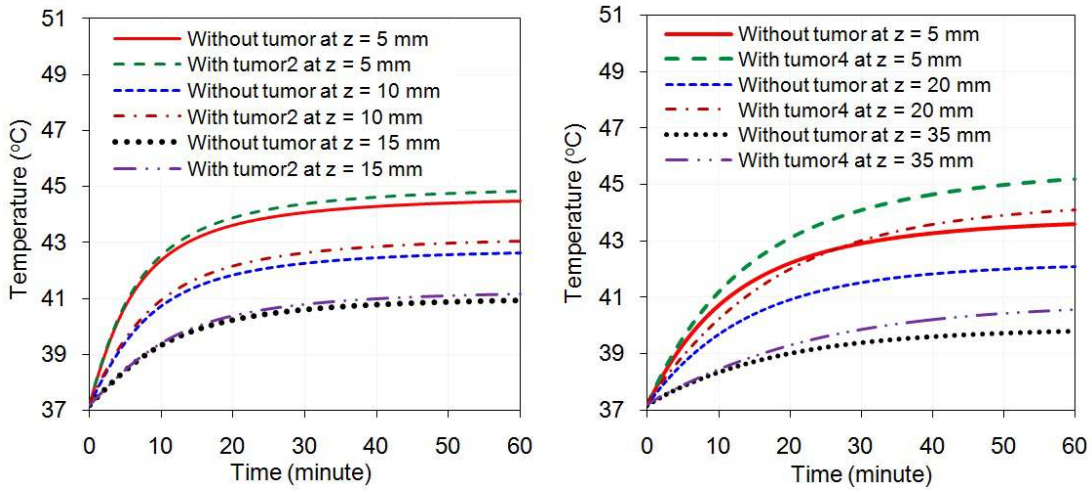

(a) (b)

Figure 4.15: Variations of temperature with time due to the MDWDHs in the realistic tri-layered bio-media without and with embedded (a) tumor2 for x = y = 0 at 2450 MHz, (b) tumor4 for x = y = 0 at 915 MHz.

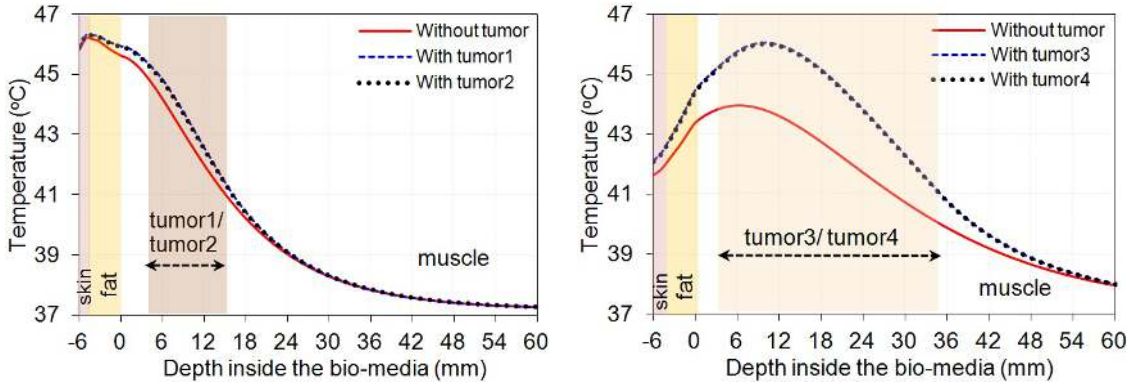

(a) (b)

Figure 4.16: Simulated temperature distributions inside the tri-layered bio-models without and with embedded tumors along z-direction (x = y = 0) due to the MDWDH at (a) 2450 MHz, and (b) 915 MHz.

Figure 4.15(a) and (b) show the variations of tissue temperature in the biological media with heating time due to the water-loaded MDWDHs designed at 2450 and 915 MHz respectively for corresponding normal bio-model without tumor and the bio-model with embedded irregular tumor (tumor2 considered at 2450 MHz and tumor4 at 915 MHz) by taking tumor depth as a parameter. It is noticed that tumor temperature in each case reaches to a higher value as compared with normal tissue temperature [Figure 4.15(a) and (b) and Table 4.3]. This would

aid in effective preferential heating of tumor in the superficial region of the body in comparison to normal tissue. Further, it can be observed from Figure 4.15(a) and (b) that initial rate of rise of temperature is higher at lower depth in the realistic tri-layered bio-media for optimum input power of 4 and 9 W respectively at the frequencies of 2450 and 915 MHz. The rate of rise of temperature in each case slows down after 40 minutes of heating and the tissue temperature approaches a steady value after about 50 minutes of heating at a given depth. The results demonstrate that tissue temperature approaches saturation after certain time period of heating at a given depth and shows decreasing trend as the depth in the medium increases.

Figure 4.16(a) and (b) shows the profiles of temperature along z-direction in the inhomogeneous tri-layered bio-media without and with embedded tumor due to the water-loaded MDWDHs designed at 2450 and 915 MHz respectively by taking tumor configuration as a parameter.

It can be observed from Figure 4.16 that temperature profiles are similar for different tumor shapes. Moreover, applicator designed at 915 MHz provides enhanced values of heating depth in the three bio-models as compared to those in the respective bio-models at 2450 MHz (Figure 4.16 and Table 4.3). Further, the depth at which temperature elevation is half of the maximum with respect to initial temperature (=$\Delta T/2$) [derived from Figures 4.16 in each case] is given in Table 4.3. Further, it is observed that the presence of tumor of one configuration or another affects to certain degree the temperature distribution along the depth at both the frequencies of interest. Also, heating of skin surface is observed using the MDWDH applicator designed at ISM frequency of 2450 MHz.

Figure 4.17(a), (b) and (c) depicts the profiles of temperature distribution in the three bio-models: bio-models without tumor, with embedded tumor1 and embedded tumor2 along x-/y-direction (y/x = 0) due to the water-loaded MDWDH designed at 2450 MHz for optimum input power of 4 W for different depths in the tumor z = 5, 10 and 15 mm respectively. Figure 4.18 (a), (b) and (c) depicts the profiles of temperature distribution in another set of three bio-models: bio-models without tumor, with embedded tumor3 and embedded tumor4 along x-/y-direction

(y/x = 0) due to the water-loaded MDWDH designed at 915 MHz for optimum input power of 9 W for different depths in the tumor z = 5, 20 and 35 mm respectively. The results show that applicators designed at 2450 and 915 MHz are able to heat effectively the respective whole tumor volume. It is to be noted that tumors (tumor3/tumor4) considered at 915 MHz are larger in size as compared with the tumors considered at 2450 MHz.

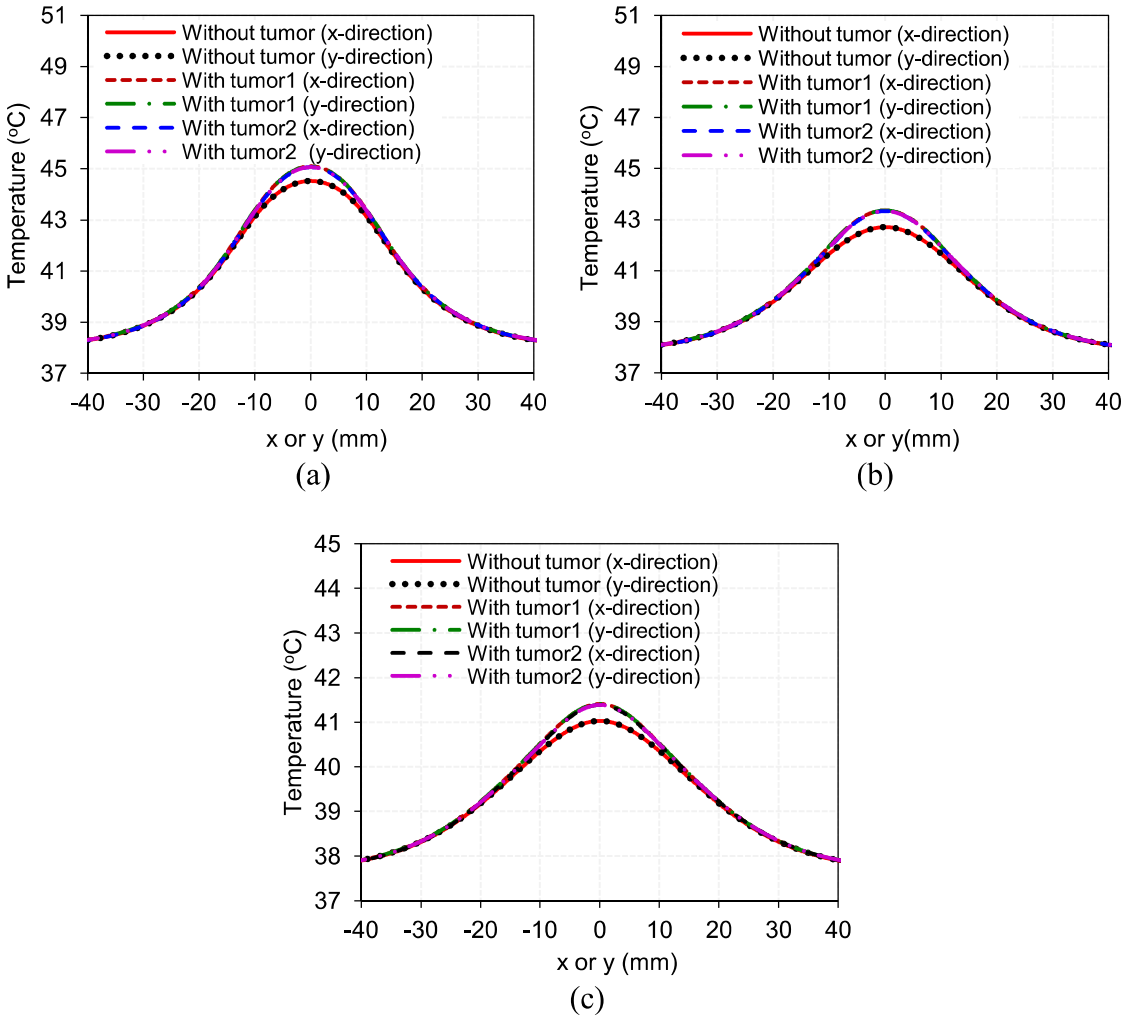

Figure 4.17: Simulated temperature distributions inside the tri-layered bio-model without tumor, with embedded tumor1 and with embedded tumor2 along x-/y-direction (y/x=0) at (b) z = 5 mm, (b) z = 10 mm, and (c) z = 15 mm, due to the MDWDH designed at 2450 MHz for 4 W input power.

Figure 4.19(a), (b), (c) and (d) shows the cross-sectional profiles of temperature distribution in the bio-media without and with tumor1/tumor2 in xz-plane (for y = 0), yz-plane (for x = 0), with embedded tumor1 in xy-plane for z = 6, 10, and 14 mm, and with embedded tumor2 in xy-plane for z = 6, 10, and 14

mm respectively owing to the water-loaded MDWDH designed at 2450 MHz. Figure 4.20(a), (b), (c) and (d) shows the cross-sectional profiles of temperature distribution in the bio-models without and with tumor3/tumor4 in xz-plane (for y =0), yz-plane (for x =0), with embedded tumor3 in xy plane for z = 6, 20, and 34 mm, and with embedded tumor4 in xy-plane for z = 6, 20, and 34 mm respectively owing to the water-loaded MDWDH designed at 915 MHz.

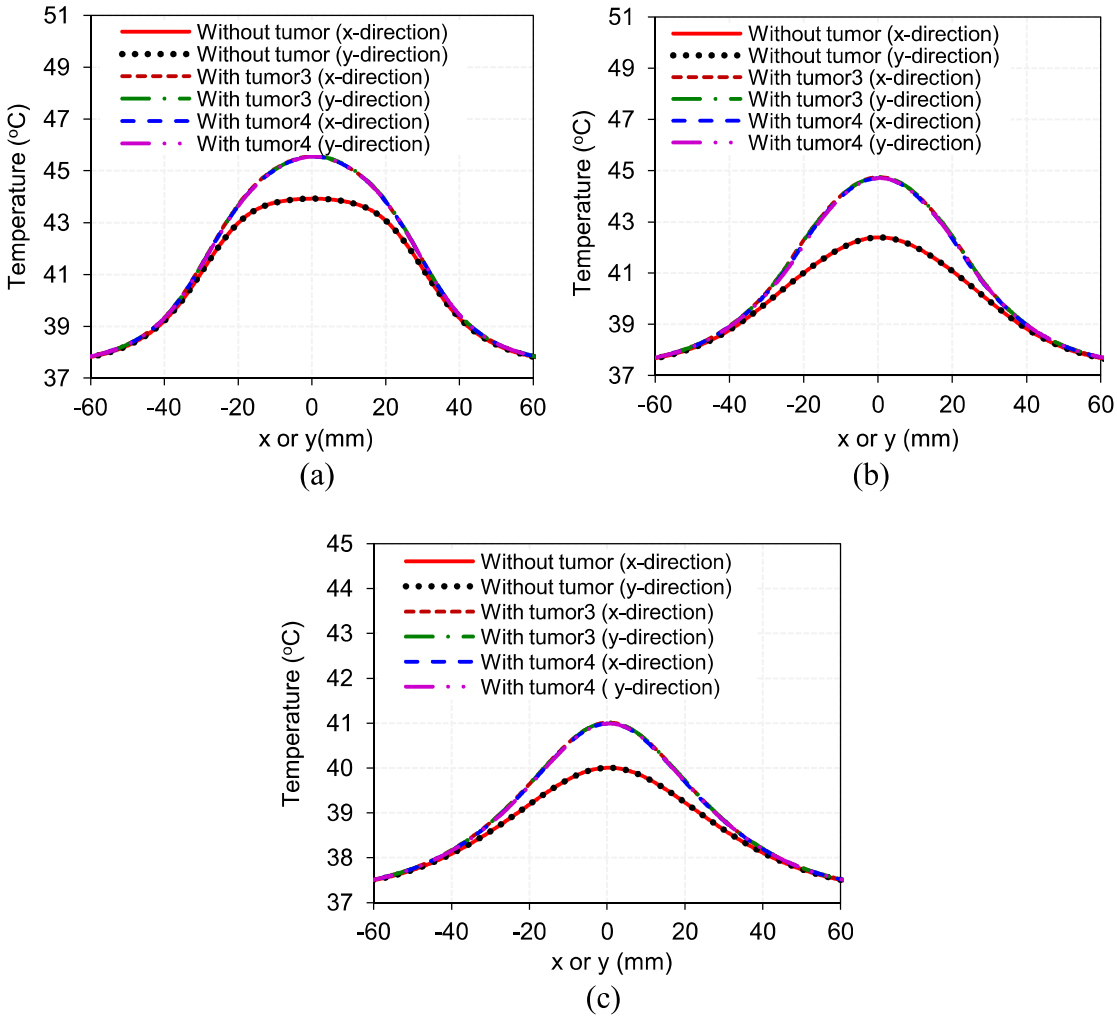

Figure 4.18: Simulated temperature distributions inside the tri-layered bio-model without tumor, with embedded tumor3, and embedded tumor4 along x-/y-direction (y/x=0) at (a) z = 5 mm, (b) z = 20 mm, and (c) z = 35 mm, due to the MDWDH designed at 915 MHz for 9 W input power.

It can be observed that antenna designed at 915 MHz provides wider heating area and enhanced heating depth in bio-models as compared with the respective parameter values at 2450 MHz. It is again apparent from Figures 4.19 and 4.20 that the respective tumors are effectively heated using the MDWDH applicators. It

can be seen that desired temperature range (41–45°C) is maintained in the respective tumors for effective hyperthermia. Further, symmetrical temperature distributions in the respective bio-media due to the MDWDH applicators are observed in the transverse xy-plane [Figures 4.19 (c), (d) and 4.20 (c), (d)].

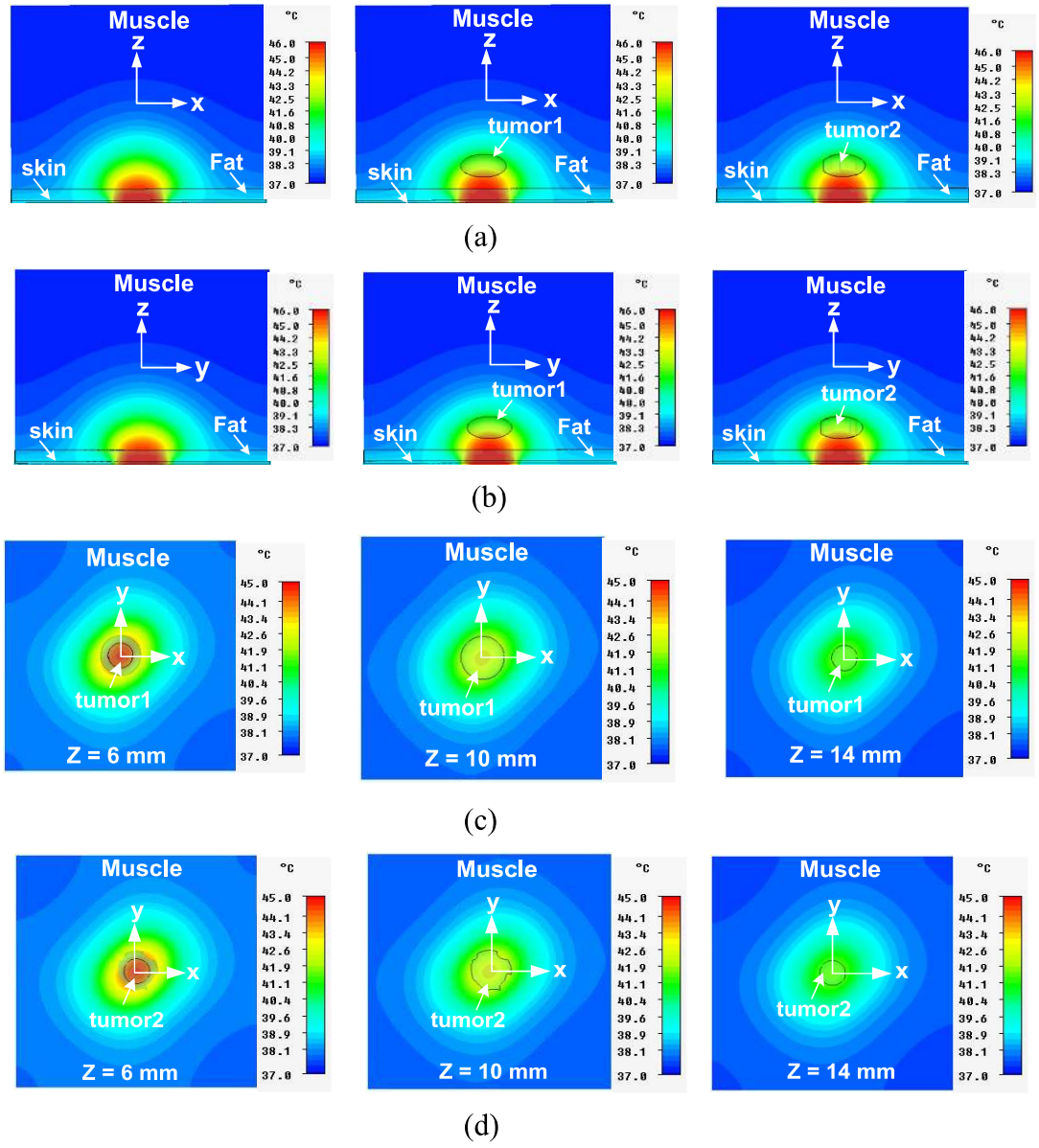

Figure 4.19: Temperature distributions inside the realistic tri-layered bio-media without and with embedded tumor1/tumor2 due to the MDWDH at 2450 MHz for 4 W input power in (a) xz-plane, (b) yz-plane, (c) xy-plane with tumor1, and (d) xy-plane with tumor2.

The values of peak temperature elevation (PTE) and the depth at which temperature elevation reduces to half of the maximum in the realistic tri-layered bio-models (obtained through thermal simulation) are also given in Table 4.3. It is

observed from Table 4.3 that presence of a tumor increases PTE in the tissue at each frequency though this increase in PTE is significant at 915 MHz. Further, the values of depth at ΔT/2 for the bio-models at 915 MHz are almost double of the respective values at 2450 MHz.

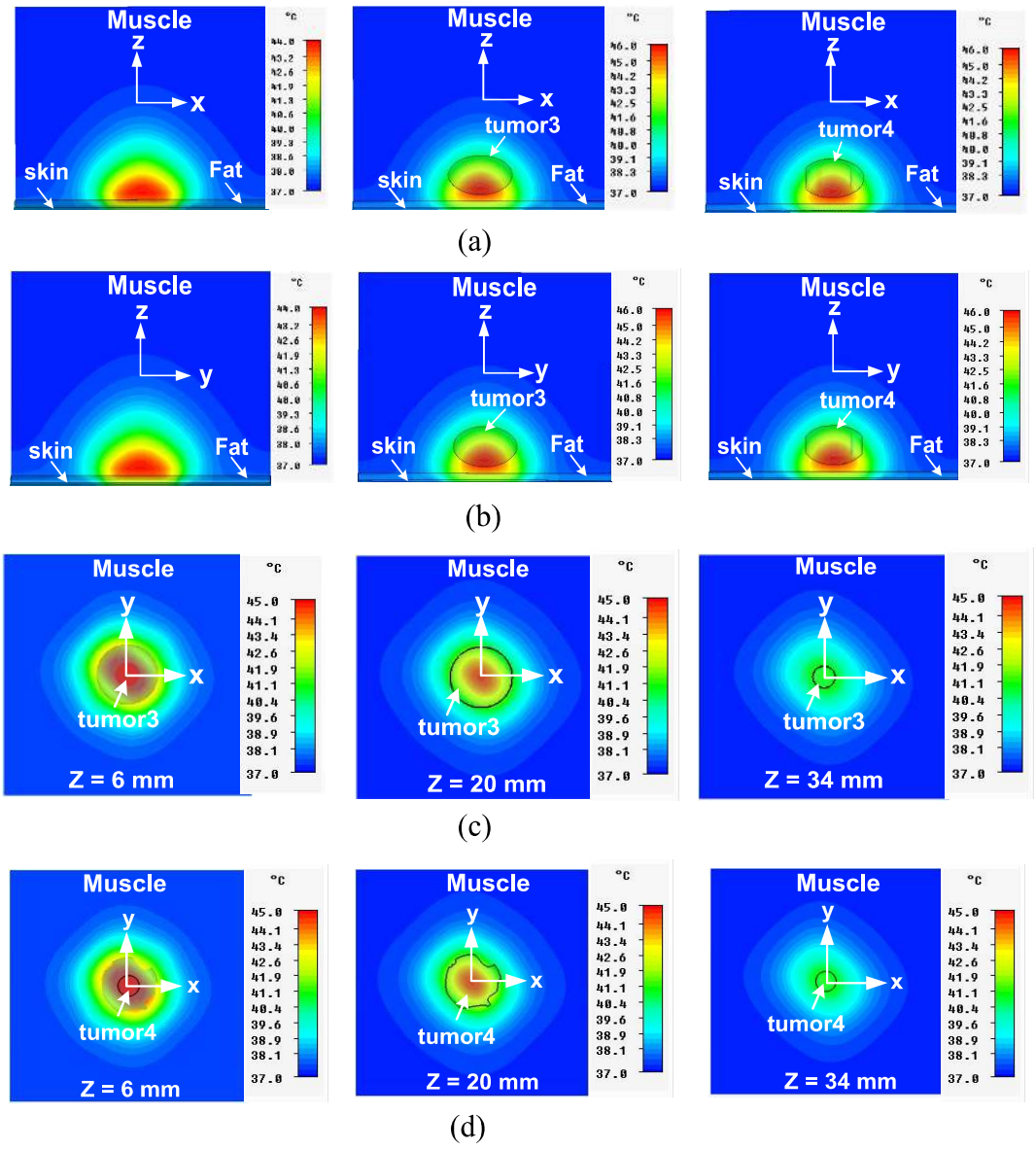

Figure 4.20: Temperature distributions inside the realistic tri-layered bio-media without and with embedded tumor3/tumor4 due to the MDWDH at 915 for 9 W input power in (a) xz-plane, (b) yz-plane, (c) xy-plane with tumor3, and (d) xy-plane with tumor4.

Finally, it can be said that oval and irregular-shaped tumors of larger size at greater depth can be effectively treated at 915 MHz as compared with 2450 MHz.

Table 4.3: Hyperthermia performance due to the water-loaded MDWDH applicators

Freq. (MHz)	Inhomogeneous model	PD (mm)	EFS[$] ($mm^2$)	PTE (^oC)	Depth at ΔT/2 (mm)	Heating area[$] {41-45$^oC$} ($mm^2$)
2450	Without tumor	15.88	27.8 × 27.8	9.22	19.12	27.1× 27.1
	With tumor1	16.2	25.87 × 25.87	9.33	20.33	28.4 × 28.4
	With tumor2	16.25	25.59 ×25.7	9.32	20.28	28.1 × 28.1
915	Without tumor	53	49 × 49	6.9	38.1	42 × 42
	With tumor3	51.7	50 × 50	9	39	52 × 52
	With tumor4	51.8	47.5 × 49.7	9	39	52.4 × 52.5

[$]EFS and heating area are defined in the middle of tumor.

4.5 Chapter summary

In the present chapter, water-loaded MDWDHs have been investigated through simulation and/or experimentally for hyperthermia application at 2450 and 915 MHz. SAR and temperature distributions in a planar biological phantom/realistic tri-layered bio-media without and with embedded oval-/irregular-shaped tumor due to the proposed MDWDHs have been determined. Results obtained through simulation and/or experimental studies indicate that the MDWDH designed at 2450 and 915 MHz gives higher PD in the homogeneous biological phantom as compared with corresponding conventional MDH. Further, the horn designed at 915 MHz and terminated in tri-layered bio-media provides higher PD and EFS as compared with those at 2450 MHz. In addition, the shape of tumor doesn't affect the PD, EFS and temperature profiles in the bio-media significantly. The diagonal horns reported in the present paper provide simple and effective means to enhance the PD in the biological models. The temperature distributions in the realistic bio-models obtained through thermal simulation indicate that the MDWDHs with 4 and 9 W input power at 2450 and 915 MHz respectively can be used as effective hyperthermia applicators for treating oval- and irregular-shaped tumors located in the abdominal/thoracic region of the body.

In the next chapter, the investigation of a conformal microstrip slot antenna integrated with artificial magnetic conductor (AMC) is presented for hyperthermia application.